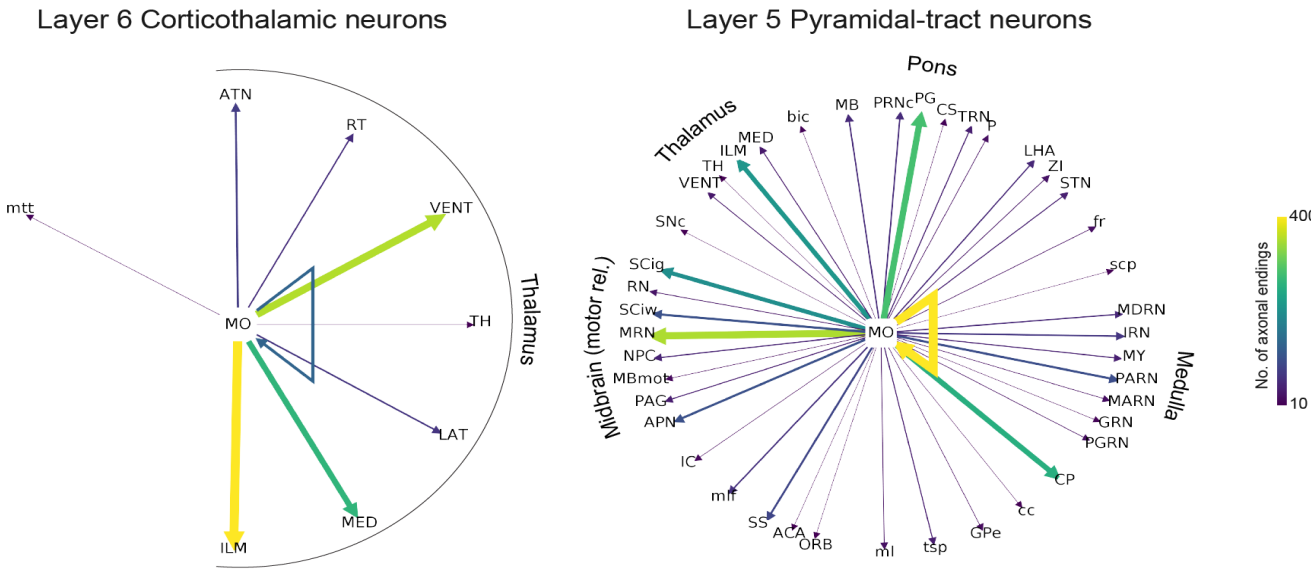

Supplementary information

SNT: a unifying toolbox for quantification of neuronal anatomy

In the format provided by the
authors and unedited



Supplementary Figure 1 | Connectivity “Ferris Wheel” diagrams for two cell populations in Layer 5/6 of the secondary motor area in the mouse brain. The two populations are described in detail in Fig. 6 of Winnubst et al.²¹. For simplicity, only brain areas at mid-ontology level (depth=6) and one morphometric criteria (no. of axonal endings at target location) were considered. The cells were retrieved from the MouseLight database and, as in **Fig. 2**, diagrams were programmatically generated (see <https://github.com/morphonets/SNTManuscript> for details). No of cells per group: 20 (corticothalamic); 14 (pyramidal-tract). Relates to Fig. 1.

Supplementary Note

Overview

SNT is an open-source (GPLv3) program written in Java and distributed with the Fiji¹ distribution of ImageJ². The source code is public and managed by git (<https://github.com/morphonets/SNT>). SNT stems from the rewrite of Simple Neurite Tracer³’s basecode following Scijava⁴ design principles and with scripting abilities inspired by several powerful open-source software for neuroanatomy, namely: L-measure⁵, nat(verse)⁶, TREES⁷, btmorph⁸, and NeuroM⁹. A special effort was put into backwards compatibility, so that SNT could supersede Simple Neurite Tracer, and remain compatible with existing Fiji plugins for neuroanatomy, namely *Sholl Analysis*¹⁰. Community-based user documentation is hosted at <https://imagej.net/SNT>.

SNT can run in headless environments, is fully scriptable and itself extensible. It inter-operates with other core components of the ImageJ ecosystem namely TrakEM2¹¹, IJ ops¹², and scenery¹³. SNT functionality can be extended using ImageJ2 commands¹⁴ or executable scripts, allowing both experienced developers and scientists with beginner-level programming experience to customize SNT. Several scripting templates are provided in Fiji’s Script Editor and a built-in discovery mechanism automatically registers user scripts in SNT’s user interface, as detailed in <https://imagej.net/SNT/> Scripting. Native Python is supported through pyimagej¹⁵. Scripting tutorials in the form of Jupyter notebooks are provided at github.com/morphonets/SNT/tree/master/notebooks.

Requirements

An up-to-date Fiji installation running Java 8 or newer. Access to “Tubular Geodesics”¹⁶ segmentation requires installation of external binaries, as described in the documentation (<https://imagej.net/SNT>). Discrete graphics card is recommended for sciview integration. VR support in sciview requires the OpenVR/SteamVR library¹³.

Installation

SNT is released through a dedicated “Neuroanatomy” update site, created to streamline and foster contributions from the wider scientific community. sciview has not been officially released and access to its functionality currently requires subscription to a second “sciview” update site. Detailed instructions are available at <https://imagej.net/SNT#Installation>.

Supported File Types

Images: SNT accepts any non-RGB image recognized by ImageJ, SCIFIO¹⁷ or Bioformats¹⁸ with up to five axes, including multi-channel and time-lapse sequences. **Neuronal reconstructions:** SNT recognizes all known variants of SWC^{19,20}, the *de facto* standard for data sharing of neuronal morphologies, MouseLight’s JSON²¹ and Simple Neurite Tracer’s TRACES open formats. **3D graphics:** Wavefront OBJ (reconstruction viewer) and STL, PLY, XYZ (sciview). **Analysis:** Output of SNT analyses can be saved as CSV (tabular data); SVG, PDF, PNG (plots, histograms and diagrams); XML (diagrams); MPG (sciview animations); and NeuroML (Cx3D models).

Supported Databases

SNT can download data directly from FlyCircuit²² (flycircuit.tw), InsectBrainDatabase (insectbraindb.org)²³, MouseLight²¹ (ml-neuronbrowser.janelia.org), NeuroMorpho²⁴ (neuromorpho.org/), and VirtualFlyBrain²⁵ (virtualflybrain.org) databases, with ongoing support for the Max Planck Zebrafish Brain Atlas²⁶ (fishatlas.neuro.mpg.de/). Data can be imported from SNT’s user interface or programmatically using its API.

Features

Semi-automated Tracing

The core of SNT’s semi-automatic reconstruction remains Simple Neurite Tracer’s exploratory approach in which the path between manually placed points along the centerline of neuronal processes is computed using bidirectional A* search³. However, several improvements were made to this procedure, namely: 1) scriptable tracing (**Fig. S1**); 2) Support for multi-channel and timelapse images (**Figs. 1, S3**); 3) refinement of centerline positioning by post-hoc fitting procedures that take into account the fluorescent signal around each traced node (**Fig. S2**); 4) Detection of signal within a local 3D neighborhood around the cursor; 5) improved synchronization mechanism of Simple Neurite Tracer’s original XY/ZY/XZ tracing views that facilitate accurate node positioning; and 6) computation of curvatures on pre-processed images. The latter allows A* to be computed on mirrored data (called a “secondary image”) in which the tube-like structures of neuronal processes have been pre-enhanced using image processing routines. For added convenience, SNT offers filtering pre-sets^{27,28} through IJ-ops¹², and allows pre-filtered data to be imported from third-party software, to e.g., allow for processing routines not yet ported into ImageJ. Adoption of other path search algorithms such as *Tubular Geodesics*¹⁶ is also possible through the installation of external binaries. Importantly, these features can be toggled at will during a tracing session.

In SNT, the accuracy and performance of the automated path search can be tuned using Hessian-based analysis of curvatures, optimized to detect tubular structures of a particular size. A key parameter of this filtering operation is σ , the size of the Gaussian kernel used to smooth the image before detection of tube-like structures occurs³. In order to provide users with sensible defaults, we ran a series of simulations to assess the impact of σ on reconstruction accuracy. For this purpose, we chose images of *Drosophila* olfactory axons from the DIADEM challenge²⁹, because these images share common acquisition parameters and their respective manual reconstructions (the “gold standards”) have been well characterized in benchmark studies. The topologies of these axons can be loosely divided into two complexity groups according to their number of branches (**Fig. S1a**). Since A* search can be scripted in SNT, these experiments were fully automated: For each cell, we iterated through the branches in the gold standard reconstruction and performed A* search between the voxels associated with the coordinates of the first and last node of each branch. This procedure was repeated while varying σ , with traced structures compared to the gold standard using the DIADEM metric³⁰ at each run.

First, we found that in the absence of human input, the simpler cells could be traced with high accuracy in the absence of Hessian pre-processing (**Fig. S1b**, median: .90/1.00 similarity score). Second, we found that under the stringent limitations of the test, Hessian pre-processing can enhance the accuracy of the segmentation of the more complex topologies (**Fig. S1c**)

but is sensitive to σ choice. It is worth noting that the default σ value—that is proposed to the user at startup upon loading of the image being traced—yielded a median DIADEM score of 0.81 for all cells combined (**Fig. S1c**). Since reconstructions associated with a score of ≥ 0.8 are considered acceptably similar^{30,31}, SNT’s default settings—that are computed on an image-per-image basis—are reasonably determined. Given that the fine-tuning of Hessian parameters is essential for accurate results, SNT provides users with an interactive widget allowing users to adjust parameters during a tracing session, as well as commands to estimate, *a priori*, the local thickness^{32,33} of the structures to be traced (**Fig. S1d**).

SNT can also execute “path fitting” routines that automatically estimate radii and the optimal position of reconstruction nodes relative to signal (**Fig. S2a**). To expedite its usage, fitting operations are undoable, and can be perused by means of

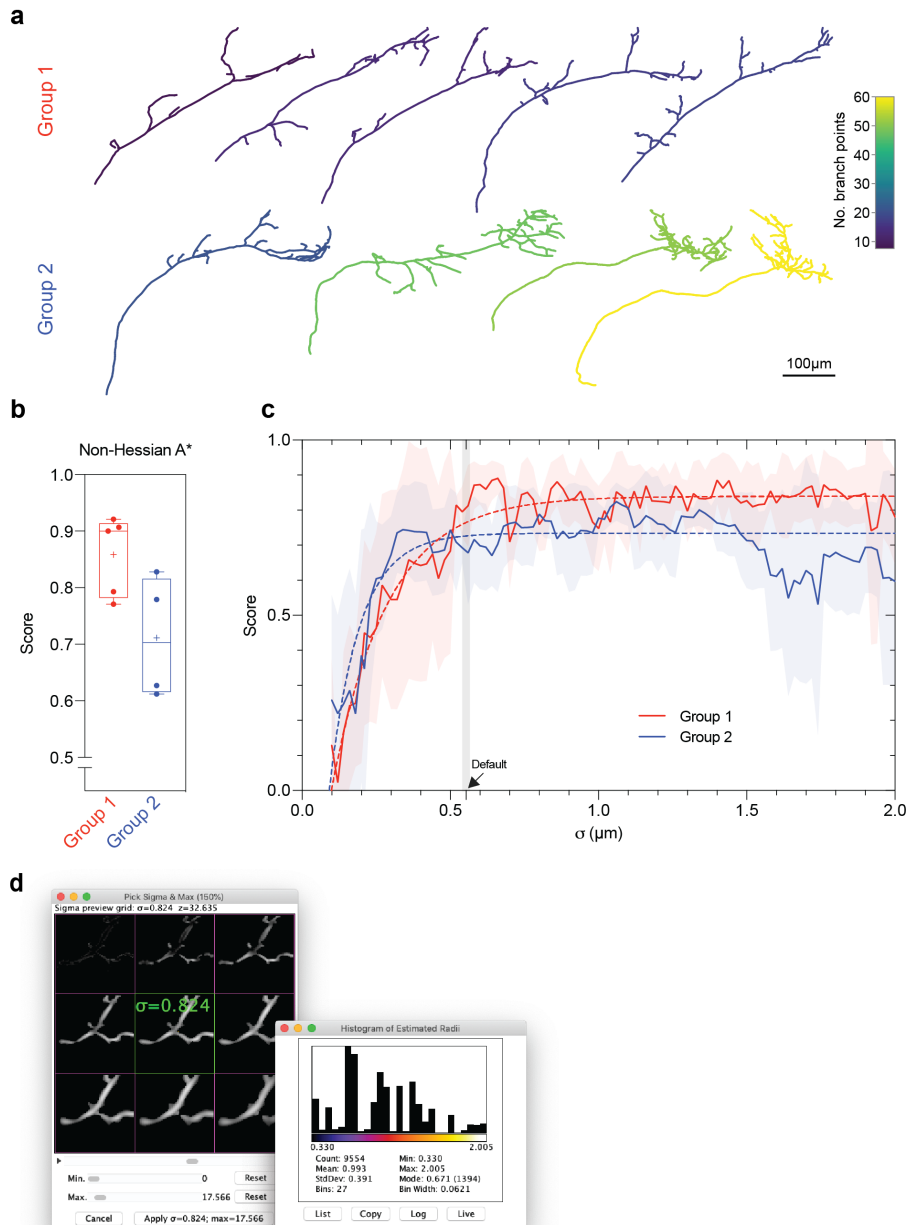


Figure S1 | Characterization of SNT’s A* tracing in fully automated tests.

(a) 2D renderings of axonal arbors of Drosophila olfactory projection neurons (DIADEM Challenge “OP” dataset) used in the tests, generated using SNT’s *Reconstruction Plotter* command. Cells are color-coded by number of branch points according to hue ramp. The 10 cells can be split into two complexity groups: ≤ 20 branches (group 1) and > 20 branches (group 2).

(b) Accuracy of automated A* without complementary Hessian analysis. Each OP cell was traced in the absence of pre-processing routines (the default in SNT) and resulting reconstruction compared to each cell’s “gold standard” using the DIADEM similarity score, in which 1 represents perfect similarity. Box depicts range between 25th and 75th percentiles. Whiskers highlight minimum and maximum. Mean marked by ‘+’. N=5 cells (group 1); 4 cells (group 2).

(c) Effect of σ on accuracy of Hessian-based A* search. For each cell, A* search was performed on Hessian-filtered data under varying σ values. As in b), resulting reconstructions were then compared to each cell’s “gold standard”. The default value that is proposed to users in SNT’s interface is indicated (arrow). Dashed lines indicate ‘best-fit’ curves (one phase exponential). N=5 cells (group 1); 4 cells (group 2), with each cell being reconstructed 95 times (95 σ values). Shaded areas depict standard deviation.

(d) SNT features several GUI-based tools that allow users to tune parameters during a tracing session. Here shown two controls for σ adjustment. Left: The “Hessian widget”, allowing interactive adjustments of σ at chosen image locations. Right: histogram of predicted radii, computed for the whole image volume being traced using local thickness analysis (depicted data for the OP_1 cell, the second most complex cell of group 2).

the “Fitting inspector” interface. SNT also allows users to identify and annotate portions of built-up topologies with colors and searchable tags based on custom labels, image data, or computed directly from morphometric traits (**Fig. S2b**).

Proof Editing and Automated Tracing

Proof-editing of automated segmentation is a major bottleneck in neuron reconstruction³⁴. To expedite the proof-editing of traced structures, SNT features an “Edit mode” in which the topology of neuronal arbors can be edited/refined with sub-pixel accuracy by means of mouse clicks or keyboard shortcuts. The ability to manipulate neuron topology is essential when attempting automated reconstructions (typically involving high contrast images of simpler, unambiguous topologies). In SNT, this procedure occurs in multiple steps: the user provides a thresholded image that is skeletonized³⁵. Such image is then internally converted into a graph-theoretic representation from which the reconstructed arbor is extracted. Similarly to other software packages³⁶, this reconstruction can then be manually edited and corrected in SNT’s graphical user interface.

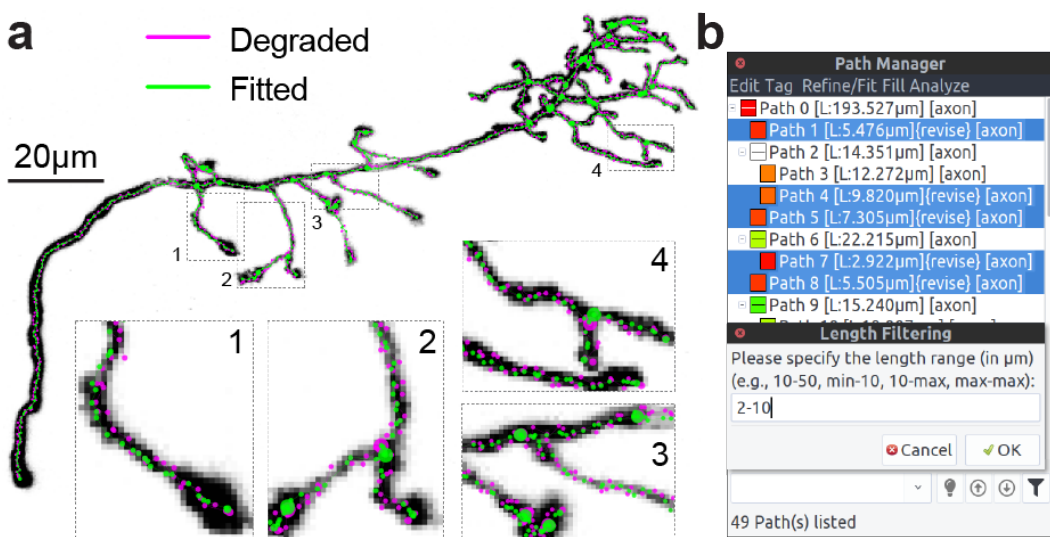


Figure S2 | Post-hoc optimization of curvatures and proof-editing tools.

(a) Refinement of node positioning through automated fitting. The “gold standard” reconstruction of the “OP_1” neuron (depicted as a Z-Projection) was programmatically degraded (magenta). Voxel intensities were used to correct degradation: SNT computed cross-sections along each traced path, ‘snapping’ nodes to their centroid, as depicted in insets. The same procedure can be used to estimate radii along the traced structure

(b) The Path Manager’s search bar provides expedite commands for annotating, filtering, and selecting paths. Such operations can be based on image data, morphometric properties or user-provided tags. These are complementary to the topology-editing commands available in “Edit Mode” (not shown).

Multidimensional Imaging

In addition to 2D and 3D images, SNT supports multi-channel and time-lapse images, up to 5 dimensions. With time-lapse imagery, SNT allows users to associate paths associated with the same neurite across frames using a two-pronged approach: 1) tags (automated and user-based) that associate paths with neurites and frames, and 2) a matching mechanism that groups paths across frames that share a common origin. The latter can occur in a lax manner to accommodate for motion artifacts across the image (**Fig. S3a**).

A key feature of SNT is seamless integration with ImageJ: Image processing routines can be inter-leaved with tracing tasks, and the entire suite of ImageJ plugins remains accessible during a tracing session. Special emphasis was put into allowing users to access image and reconstructed data in convenient ways. For example, reconstructed paths can be converted into functional ROIs and voxel intensities profiled along their center-lines. With multi-color fluorescence microscopy producing

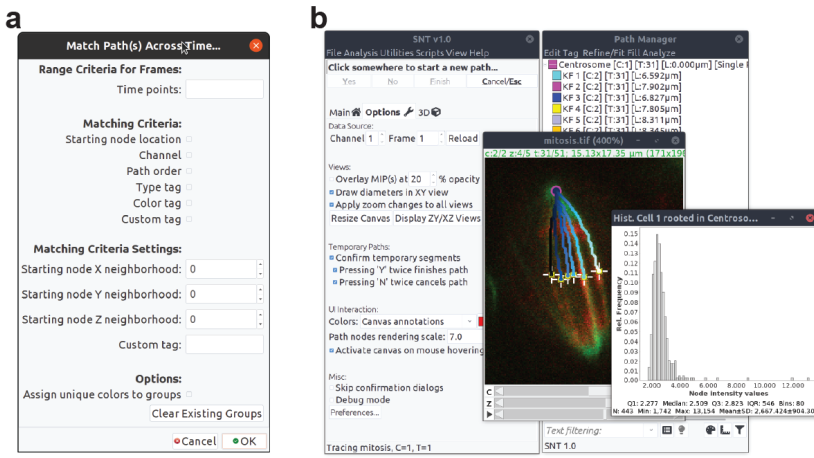


Figure S3 | Analysis of 4D and 5D imagery.

a) Time-lapse Analyses: Dialog of the “Match Path(s) Across Time” command showcasing the options for matching paths across time so that they remain associated with their common dendrite. The command is part of the “Time-lapse Utilities” that allow for morphometric time profiles (Fig. 1b).

b) Analysis of non-neuronal imagery. K-fibers were traced during anaphase in a multi-channel 3D timelapse of dividing S2 cells⁵³ (IJ1 “mitosis” 5D sample image). Traces were color-coded uniquely, according to their location along the X- axis. Histogram depicts how the voxel data underlying traced data can be easily accessed from built-in commands. Conversion of tracings into functional ImageJ ROIs is also easily accomplished, as exemplified by point ROIs (“+” markers) highlighting chromosome-attachment sites.

multi-channel images, this functionality allows users to quantify fluorescent signal along traced structures, and measure the signal from other probes in the imaged tissue (Fig. 1c). Although such features are of proven utility for many types of data (Fig. S3), we anticipate immediate utility in studies focused on neuroregeneration and neuron-glia interactions, in which the cellular environments around neurons is imaged and analyzed.

Visualization and Analysis

For simplified visualization of single-cell data SNT implements “Reconstruction Plotter”, a two-dimensional (2D) canvas for vector-based plotting of reconstructions (Fig. S1a). The main advantage of this type of viewer is that reconstructions can be scaled up or down to any resolution without being affected by aliasing artifacts. However, it can only render 2D data. For rendering more complex 3D data, SNT features two additional viewers: *Reconstruction Viewer* and sciview¹³.

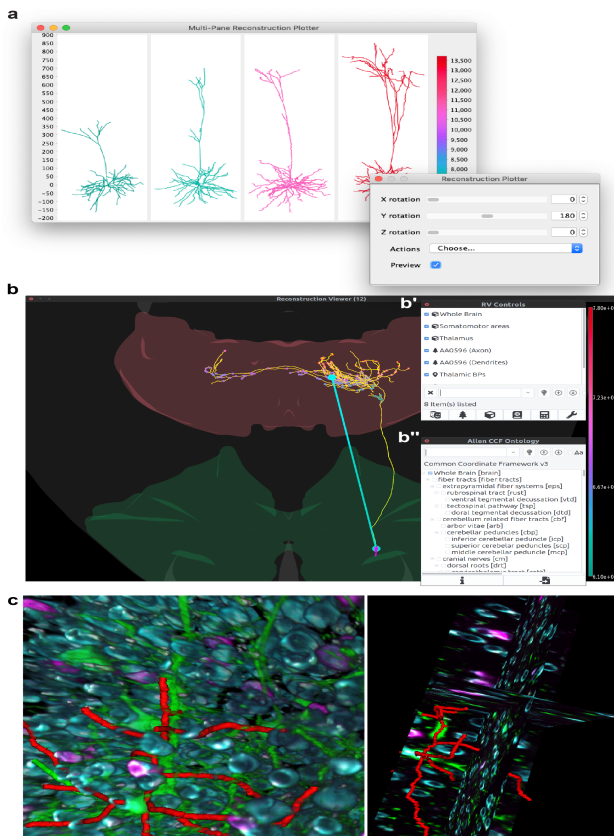


Figure S4 | Neuroanatomy viewers.

(a) *Reconstruction Plotter* assembles multi-panel 2D plots of reconstructed cells. Here, four dendritic arbors from the MouseLight database (IDs AA001–4), were automatically aligned, ranked and color-coded by cable length. When called from the GUI (graphical user interface), data can be transformed interactively (inset). Axis and scale bar in μm .

(b) *Reconstruction Viewer* (RV) is a 3D visualization tool designed to handle neuroanatomy exclusively. Transverse view of the mouse brain, depicting a MouseLight pyramidal cell (ID AA0596; axon in yellow, dendrites in magenta) in the motor cortex (green). All axonal branch points within the Thalamus (red) have been identified and color-coded by depth, as per hue ramp. The vector connecting the cell soma to the centroid of thalamic branch points is highlighted. RV Controls (b') are organized in a layout modeled after *Path Manager* (Fig. S2b) in SNT’s tracing interface. Extra functionality, such as access to Allen CCF ontologies (b'') is provided through dedicated dialogs.

(c) sciview integration allows SNT data to be rendered with arbitrarily large image volumes. Left: Surface visualization of the multi-channel volume described in Fig. 1 (reconstructed dendrites in red). Right: Ortho-view of the same data (experimental feature at the time of this writing). For clarity, components of the sciview user interface (scene inspector, interactive scripting shell, Cx3D bridge, etc.) were omitted.

Reconstruction Viewer (RV) is hardware accelerated, supporting both surface meshes and reconstruction files (**Fig. S4b**). The viewer can render both local and remote files on the same scene, which allows for direct loading of reconstructions from all of the supported databases and meshes for several template brains, i.e.: Drosophila (larval and adult) via Virtual Fly Brain, FlyLight, and FlyCircuit^{22,25,37}; Allen Mouse Brain Common Coordinate Framework^{38,39} (CCF, adult mouse) via MouseLight database²¹; and Zebrafish via the Max Planck Zebrafish Brain Atlas²⁶. In the case of the Allen Mouse Brain Atlas³⁹, the full stack of anatomical ontologies is supported (**Fig. S4b'**). Reconstruction Viewer can also be used as a stand-alone application (i.e., in the absence of SNT's tracing interface), allowing it to be accessed from other environments such as IPython. All Reconstruction Viewer instances can be scripted once displayed, and can be instantiated in “high-performance” mode, suitable for visualization of large amounts of data. As a proof-of-principle we used this feature to visualize the entire MouseLight database on a laptop computer without a discrete graphics card (**Sup. Video 1**). Another key feature of Reconstruction Viewer is its ability to perform geometric analyses on both meshes and reconstructions, which is key for studying the topographic organization of neurons across neuropils (**Fig. S4b**).

sciview is a powerful SciJava-based visualization tool for volumetric and mesh-based data (**Fig. S4c**, **Sup. Video 2**). sciview has been recently improved to support out-of-core volume rendering of images up to 9.261×10^{27} voxels¹³ (via BigDataViewer⁴⁰), making it an appealing choice for visualization of large imagery.

SNT analytical capabilities are three-fold: 1) Analysis of imagery data already discussed; 2) Morphometric analysis of single cells in isolation and 3) Analysis of groups of cells in a common, annotated space (a reference brain/neuropil), which requires handling of neuroanatomical volumes. For morphometric analyses, SNT supports commonly used metrics⁵, graph theory based analysis, and popular quantification strategies, such as Sholl¹⁰ and Strahler^{41–43}. In addition, SNT's API allows for analyses based on persistent homology^{44,45} (including persistence landscapes⁴⁶) and other ad-hoc statistical measurements complementary to those available through the user interface (**Fig. S5**).

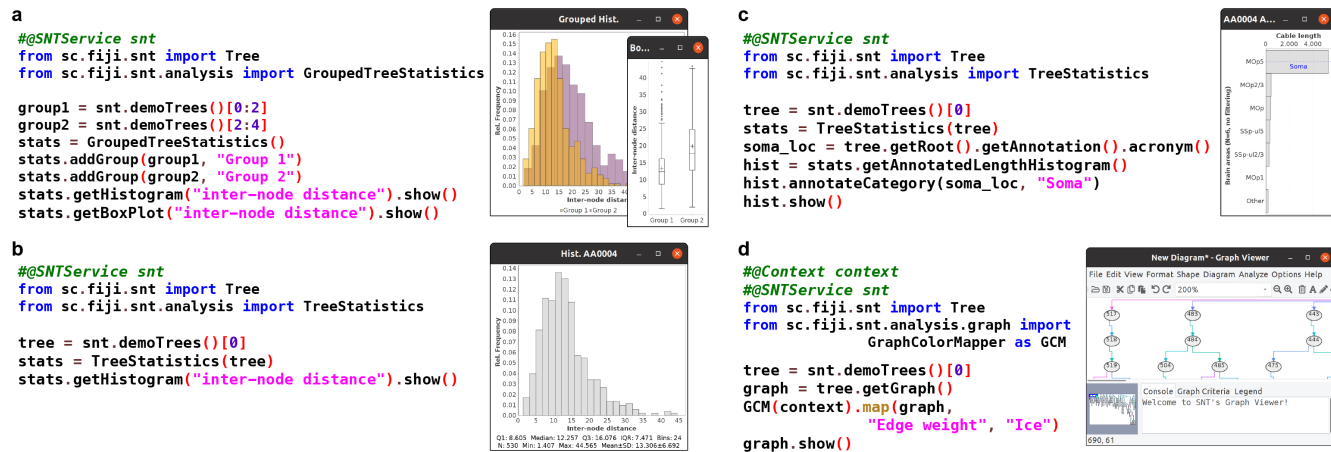


Figure S5 | Overview of analysis API.

Functional scripts (written in Python) showcasing SNT's API (application programming interface) on dendritic arbors from the MouseLight database (cells IDs AA0001–4) that can be access offline from within SNT as “demo trees”. For each panel, the script code (as typed in Fiji's script editor) is showed on the left. Script's output on the right.

(a,b) Statistics of morphometric traits can be extracted from groups of neurons (a), a single neuron (b), or parts thereof (not shown). Convenience methods allow data to be output in histograms, plots and tables. (c) Distribution of cable length across brain areas of the cell's neuropil, in this case compartments from the Allen Mouse CCF. (d) Neuronal reconstructions can be converted to graphs succinctly, programmatically annotated and displayed in SNT's interactive *Graph Viewer*. This code snippet also demonstrates how SNT interacts with the SciJava⁴ API.

Modeling

Cortex3D (Cx3D) is a computational modeling tool for simulating neurodevelopmental processes⁴⁷ and has been used to define generative models of cortical circuits⁴⁸. We integrate Cx3D with SNT through the sciview visualization package by rewriting Cx3D to grow neuronal processes with sciview's data structures. This facilitates the use of both SNT's and

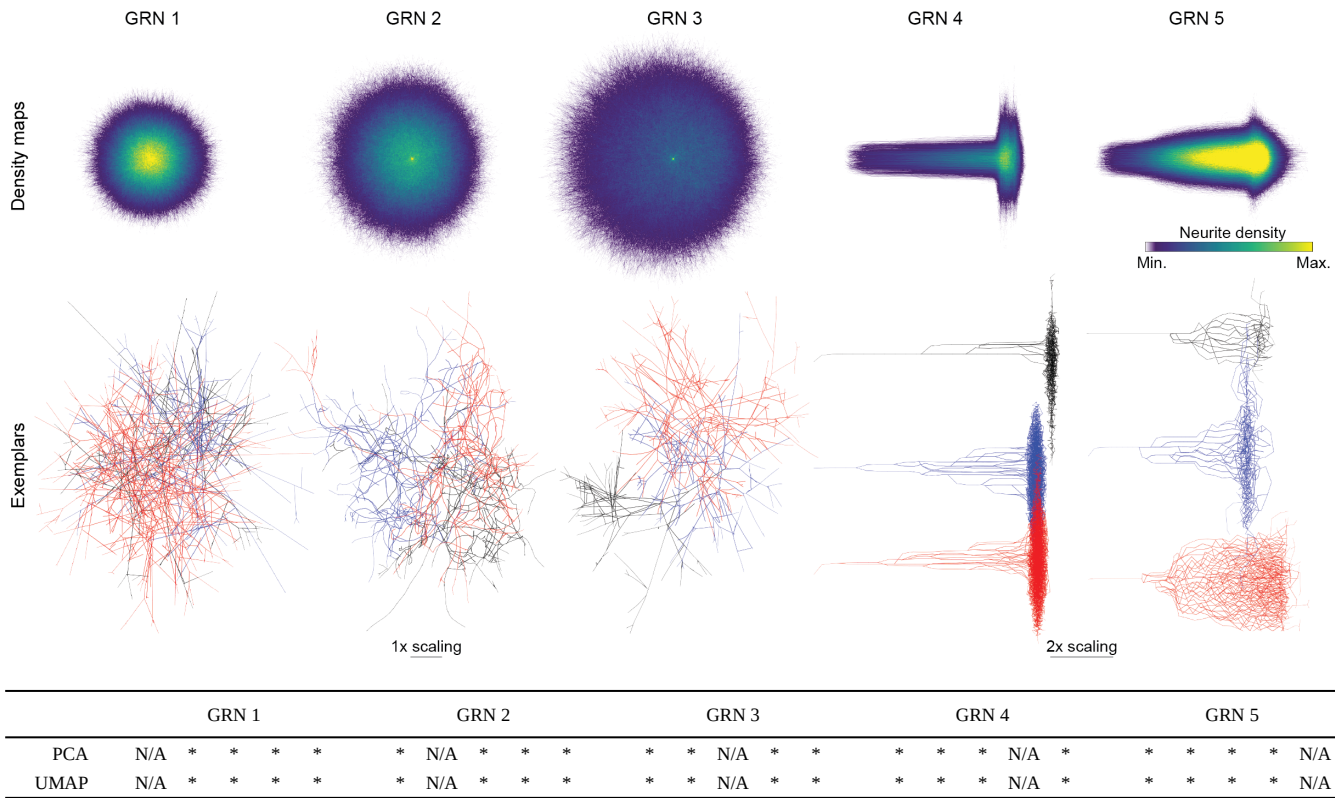


Figure S6 | Statistical discrimination between morphological populations of cells generated *in silico*.

Top: Density maps for the five neurodevelopmental cell types artificially generated using unique GRNs, obtained by overlaying all soma-aligned cells in the group. Color coding reflects the density of neurites at a given location for the 5 groups.

Middle: Representative exemplars of each group. For clarity, cells from GRNs 4 and 5 were separated by a vertical offset.

Bottom: Summary of pairwise statistical measures of morphological differences between the five groups analyzed under different dimensionality reduction techniques. Principal components, t-SNE features (not shown) and UMAP components were computed from default SNT metrics and compared using a modified two-sample Kolmogorov Smirnov test. *: $p < 0.001$; N/A: no test performed between same sample. Computed results available at <https://github.com/morphonets/SNTManuscript>.

Cells from GRNs 4 and 5 were re-scaled in top and middle panel so that all cells could be rendered under equivalent dimensions. $N=1000$ cells per group.

ImageJ's functionality when designing Cx3D models. We present two important examples that benefit from the unification of quantitative neuroanatomy and morphological modeling: statistical discrimination between morphological cell types, and image-based modeling of neural morphologies. However, there are many additional possibilities enabled by this coupling, from generative testing of new quantitative measurements to data-driven model fitting.

Morphological Discrimination Between Cell Types

Morphological discrimination between neuronal cell types is an important aspect of cell classification. The quantitative measurements made by SNT can be used to statistically test the difference between morphological populations of cells. To test this, we generated thousands of unique artificial neurons that 'developed' *in silico* under similar conditions and asked if SNT metrics could resolve such morphologically-related topologies.

First we integrated a computational model of artificial gene regulatory networks (GRNs)⁴⁹ into Cx3D for the control of cellular processes. An overview of the GRN architecture and mechanism of simulating GRN dynamics is described in detail in the previous publication⁴⁹. Second, we generated five unique GRNs. While each of the five unique GRNs are randomly

generated, all GRNs are provided with common inputs: directional cues for each 3-dimensional axis, length of the neurite segment, volume of the neurite segment, and local branch order. Additionally, all GRNs have common outputs: directional bias for each 3-dimensional axis, directional bias for previous direction of growth, directional bias for taking a random direction, a factor for increasing the segmentation of a neurite, and a factor for increasing the probability of branching. This type of input/output behavior is described extensively in previous publications of the Cx3D simulator^{47,48}. The specific connectivity and number of regulatory components of the GRN were randomized. However, completely randomized GRNs have a low probability of being capable of generating viable morphologies. To address this, rejection sampling was used when generating the random GRNs by testing that each network satisfied a minimal viability criteria. The viability test was performed as follows: the GRN is simulated for 100 time-steps with constant input values, with the following criteria assessed at the first and final time-step of the viability test: (1) all behavior regulating protein concentrations should change, (2) the GRN must bifurcate enough to have reasonable growth, (3) the GRN must not over-bifurcate, (4) the GRN must trigger branching, and (5) the GRN must not overbranch. While these criteria will have an impact on the distribution of possible GRNs that are selected, the rationale for this approach is to compensate for the fact that most randomly generated GRNs are not capable of generating physically plausible neurodevelopment.

For each GRN, we stochastically generated 1,000 artificial neurons—under the same environmental conditions—and analyzed their skeletons with SNT core metrics (**Fig. S6**). We then performed Principal Component Analysis (PCA) and statistically tested the difference between principal components with two-sample Kolmogorov-Smirnov tests combined with the Fisher combined probability test (**Methods**). We obtained statistical significance on all comparisons. All groups were similarly resolved when extending this approach to other dimensionality reduction techniques (t-SNE⁵⁰ and UMAP⁵¹).

Image-based Modeling

By unifying SNT and Cx3D, we can leverage ImageJ within Cx3D to enable support for image-based modeling. We demonstrate a proof-of-concept simulation based upon an *in vitro* microfluidic assay designed for screening the effect of chemoattractants on neuronal growth⁵². We recreated their microfluidic circuit topology as a 3-dimensional image, and define gradients of chemoattractant using intensity values of the image voxels, analogous to the original experiment's Netrin assay. Neurite outgrowths follow chemical gradients of increasing concentration defined within the microfluidic circuit. We show a simulated neuron and image-based environment in **Sup. Video 3**.

The neurodevelopment model encodes a minimal artificial environment reminiscent of an *in vitro* assay. A neuron is initialized as a single soma at a randomly selected position within +/- 40 spatial units of the origin (0, 0, 0) along the X-, Y-, and Z- axes. Three extracellular morphogen gradients are established and extend for 300 spatial units along the three axes in a Gaussian distribution concentration. The simulation begins by extending an initial neurite segment from the soma. The GRNs then regulate the growth of neurites with the previously described inputs and outputs. The model proceeds by iteratively simulating physical constraints encoded in the Cx3D simulation engine and the dynamics of the GRN to grow the artificial neuron.

Glossary

GRNs Artificial gene regulatory networks (GRNs) are mathematical algorithms inspired by mechanisms of biological gene regulation. GRNs can be used to model or solve problems with a strong dynamic or stochastic component

Mesh A polygon mesh defines the shape of a three-dimensional polyhedral object. In neuronal anatomy, meshes define *neuropil* annotations, typically compartments of a reference brain atlas (e.g., the hippocampal formation in mammals, or mushroom bodies in insects)

Multi-dimensional image An image with more than 3 dimensions (3D). Examples include fluorescent images associated with multiple fluorophores (multi-channel) and images with a time-dimension (time-lapse videos). A 3D multi-channel timelapse has 5 dimensions

Neurite Same as neuronal process. Either an axon or a dendrite

Path Can be defined as a sequence of branches, starting from soma or a branch point until a termination. In manual and assisted (semi-automated) tracing, neuronal arbors are traced using paths, not branches. Fitting algorithms that take into account voxel intensities can be used to refine the center-line coordinates of a path, typically to obtain more accurate curvatures. Fitting procedures can also be used to estimate the volume of the neurite(s) associated with a path

(Neuronal) morphometry Quantification of neuronal morphology

Neuropil Any area in the nervous system. The cellular tissue around neuronal processes

Out-of-core Software with *out-of-core* capabilities is able to process data that is too large to fit into a computer's main memory

Reconstruction See *Tracing*

ROI Region of Interest. Define specific parts of an image to be processed in image processing routines

Skeleton A thinned version of a digitized shape (such as a neuronal reconstruction) or of a binary image

Tracing A digital reconstruction of a neuron or neurite. The term predates computational neuroscience and reflects the manual 'tracing' on paper performed with camera lucida devices by early neuroanatomists

Volume rendering A visualization technique for displaying image volumes (3D images) directly as 3D objects

References

1. Schindelin, J. *et al.* Fiji: an open-source platform for biological-image analysis. *Nat. Methods* **9**, 676–682 (2012).
2. Schneider, C. A., Rasband, W. S. & Eliceiri, K. W. NIH Image to ImageJ: 25 years of image analysis. *Nat. Methods* **9**, 671–675 (2012).
3. Longair, M. H., Baker, D. A. & Armstrong, J. D. Simple Neurite Tracer: open source software for reconstruction, visualization and analysis of neuronal processes. *Bioinformatics* **27**, 2453–2454 (2011).
4. Rueden, C., Schindelin, J., Hiner, M. C. & Eliceiri, K. *SciJava Common [Software]*. <http://scijava.org/>.
5. Scorcioni, R., Polavaram, S. & Ascoli, G. A. L-Measure: a web-accessible tool for the analysis, comparison and search of digital reconstructions of neuronal morphologies. *Nat. Protoc.* **3**, 866–876 (2008).
6. Bates, A. S. *et al.* The natverse, a versatile toolbox for combining and analysing neuroanatomical data. *eLife* **9**, e53350 (2020).
7. Cuntz, H., Forstner, F., Borst, A. & Häusser, M. One Rule to Grow Them All: A General Theory of Neuronal Branching and Its Practical Application. *PLOS Comput. Biol.* **6**, e1000877 (2010).
8. Torben-Nielsen, B. An Efficient and Extendable Python Library to Analyze Neuronal Morphologies. *Neuroinformatics* **12**, 619–622 (2014).
9. Juan Palacios *et al.* BlueBrain/NeuroM. (Zenodo, 2020). doi:10.5281/zenodo.597333.
10. Ferreira, T. A. *et al.* Neuronal morphometry directly from bitmap images. *Nat. Methods* **11**, 982–984 (2014).
11. Cardona, A. *et al.* TrakEM2 Software for Neural Circuit Reconstruction. *PLOS ONE* **7**, e38011 (2012).
12. Rueden, C. *et al.* *ImageJ Ops [Software]*. <http://imagej.net/Ops>. (2016).
13. Günther, U. *et al.* scenery: Flexible Virtual Reality Visualization on the Java VM. *ArXiv190606726 Cs* (2019).
14. Rueden, C. T. *et al.* ImageJ2: ImageJ for the next generation of scientific image data. *BMC Bioinformatics* **18**, 529 (2017).
15. *pyimagej [Software]*. <https://github.com/imagej/pyimagej>.
16. Türetken, E., Benmansour, F. & Fua, P. Automated reconstruction of tree structures using path classifiers and Mixed Integer Programming. in *2012 IEEE Conference on Computer Vision and Pattern Recognition* 566–573 (2012). doi:10.1109/CVPR.2012.6247722.
17. Hiner, M. C., Rueden, C. T. & Eliceiri, K. W. SCIFIO: an extensible framework to support scientific image formats. *BMC Bioinformatics* **17**, 521 (2016).
18. Linkert, M. *et al.* Metadata matters: access to image data in the real world. *J. Cell Biol.* **189**, 777–782 (2010).
19. Cannon, R. C., Turner, D. A., Pyapali, G. K. & Wheal, H. V. An on-line archive of reconstructed hippocampal neurons. *J. Neurosci. Methods* **84**, 49–54 (1998).
20. Nanda, S. *et al.* Design and implementation of multi-signal and time-varying neural reconstructions. *Sci. Data* **5**, 170207 (2018).
21. Winnubst, J. *et al.* Reconstruction of 1,000 Projection Neurons Reveals New Cell Types and Organization of Long-Range Connectivity in the Mouse Brain. *Cell* **179**, 268–281.e13 (2019).
22. Chiang, A.-S. *et al.* Three-dimensional reconstruction of brain-wide wiring networks in Drosophila at single-cell resolution. *Curr. Biol. CB* **21**, 1–11 (2011).
23. Heinze, S. *et al.* InsectBrainDatabase - A unified platform to manage, share, and archive morphological and functional data. *bioRxiv* 2020.11.30.397489 (2020) doi:10.1101/ghng96.
24. Ascoli, G. A., Donohue, D. E. & Halavi, M. NeuroMorpho.Org: A Central Resource for Neuronal Morphologies. *J. Neurosci.* **27**, 9247–9251 (2007).
25. Miliyaev, N. *et al.* The Virtual Fly Brain browser and query interface. *Bioinforma. Oxf. Engl.* **28**, 411–415 (2012).
26. Kunst, M. *et al.* A Cellular-Resolution Atlas of the Larval Zebrafish Brain. *Neuron* (2019) doi:10.1016/j.neuron.2019.04.034.
27. Frangi, A. F., Niessen, W. J., Vincken, K. L. & Viergever, M. A. Multiscale vessel enhancement filtering. in *Medical Image Computing and Computer-Assisted Intervention — MICCAI'98* (eds. Wells, W. M., Colchester, A. & Delp, S.) vol. 1496 130–137 (Springer Berlin Heidelberg, 1998).
28. *Tubeness [Software]*. <https://imagej.net/Tubeness>.
29. Brown, K. M. *et al.* The DIADEM Data Sets: Representative Light Microscopy Images of Neuronal Morphology to Advance Automation of Digital Reconstructions. *Neuroinformatics* **9**, 143–157 (2011).
30. Gillette, T. A., Brown, K. M. & Ascoli, G. A. The DIADEM Metric: Comparing Multiple Reconstructions of the Same Neuron. *Neuroinformatics* **9**, 233–245 (2011).
31. Usher, W. *et al.* A Virtual Reality Visualization Tool for Neuron Tracing. *IEEE Trans. Vis. Comput. Graph.* **24**, 994–1003 (2018).
32. Hildebrand, T. & Rüegsegger, P. A new method for the model-independent assessment of thickness in three-dimensional

- images. *J. Microsc.* **185**, 67–75 (1997).
33. *Local Thickness [Software]*. https://imagej.net/Local_Thickness.
34. Peng, H., Long, F., Zhao, T. & Myers, E. Proof-editing is the Bottleneck Of 3D Neuron Reconstruction: The Problem and Solutions. *Neuroinformatics* **9**, 103–105 (2011).
35. Arganda-Carreras, I., Fernández-González, R., Muñoz-Barrutia, A. & Ortiz-De-Solorzano, C. 3D reconstruction of histological sections: Application to mammary gland tissue. *Microsc. Res. Tech.* **73**, 1019–1029 (2010).
36. Feng, L., Zhao, T. & Kim, J. neuTube 1.0: A New Design for Efficient Neuron Reconstruction Software Based on the SWC Format. *eNeuro* **2**, (2015).
37. Jenett, A. *et al.* A GAL4-Driver Line Resource for Drosophila Neurobiology. *Cell Rep.* **2**, 991–1001 (2012).
38. Wang, Q. *et al.* The Allen Mouse Brain Common Coordinate Framework: A 3D Reference Atlas. *Cell* **181**, 936–953.e20 (2020).
39. Lein, E. S. *et al.* Genome-wide atlas of gene expression in the adult mouse brain. *Nature* **445**, 168–176 (2007).
40. Pietzsch, T., Saalfeld, S., Preibisch, S. & Tomancak, P. BigDataViewer: visualization and processing for large image data sets. *Nat. Methods* **12**, 481–483 (2015).
41. Horton, R. E. Erosional Development Of Streams And Their Drainage Basins: Hydrophysical Approach To Quantitative Morphology. *GSA Bull.* **56**, 275–370 (1945).
42. Strahler, A. N. Quantitative analysis of watershed geomorphology. *Trans. Am. Geophys. Union* **38**, 913 (1957).
43. Vormberg, A., Effenberger, F., Muellerleile, J. & Cuntz, H. Universal features of dendrites through centripetal branch ordering. *PLOS Comput. Biol.* **13**, e1005615 (2017).
44. Li, Y., Wang, D., Ascoli, G. A., Mitra, P. & Wang, Y. Metrics for comparing neuronal tree shapes based on persistent homology. *PLOS ONE* **12**, e0182184 (2017).
45. Kanari, L. *et al.* A Topological Representation of Branching Neuronal Morphologies. *Neuroinformatics* **16**, 3–13 (2018).
46. Bubenik, P. Statistical Topological Data Analysis using Persistence Landscapes. *26*.
47. Zubler, F. & Douglas, R. A framework for modeling the growth and development of neurons and networks. *Front. Comput. Neurosci.* **3**, 25 (2009).
48. Zubler, F. *et al.* Simulating Cortical Development as a Self Constructing Process: A Novel Multi-Scale Approach Combining Molecular and Physical Aspects. *PLOS Comput. Biol.* **9**, 1–15 (2013).
49. Cussat-Blanc, S., Harrington, K. & Pollack, J. Gene Regulatory Network Evolution Through Augmenting Topologies. *IEEE Trans. Evol. Comput.* **19**, 823–837 (2015).
50. Maaten, L. van der & Hinton, G. Visualizing Data using t-SNE. *J. Mach. Learn. Res.* **9**, 2579–2605 (2008).
51. McInnes, L., Healy, J. & Melville, J. UMAP: Uniform Manifold Approximation and Projection for Dimension Reduction. *ArXiv180203426 Cs Stat* (2018).
52. Kothapalli, C. R. *et al.* A high-throughput microfluidic assay to study neurite response to growth factor gradients. *Lab. Chip* **11**, 497–507 (2011).
53. Vale, R. D., Spudich, J. A. & Griffis, E. R. Dynamics of myosin, microtubules, and Kinesin-6 at the cortex during cytokinesis in Drosophila S2 cells. *J. Cell Biol.* **186**, 727–738 (2009).